Journal of Colloid and Interface Science 607 (2022) 1226–1238

Contents lists available at ScienceDirect

Journal of Colloid and Interface Science

journal homepage: www.elsevier.com/locate/jcis

Zeta potential of CO_2-rich aqueous solutions in contact with intact sandstone sample at temperatures of 23 °C and 40 °C and pressures up to 10.0 MPa

Miftah Hidayat [a,b], Mohammad Sarmadivaleh [b], Jos Derksen [a], David Vega-Maza [a,c], Stefan Iglauer [d,e], Jan Vinogradov [a,*]

[a] University of Aberdeen, School of Engineering, Elphinstone Road, AB24 3UE Aberdeen, United Kingdom
[b] Curtin University, Discipline of Petroleum Engineering, 26 Dick Perry Avenue, 6151 Kensington, Australia
[c] Now at University of Valladolid, School of Engineering. TermoCal, BioEcoUva Institute, Valladolid, Spain
[d] Edith Cowan University, Centre for Sustainable Energy and Resources, 270 Joondalup Drive, 6027 Joondalup, Australia
[e] Edith Cowan University, School of Engineering, 270 Joondalup Drive, 6027 Joondalup, Australia

GRAPHICAL ABSTRACT

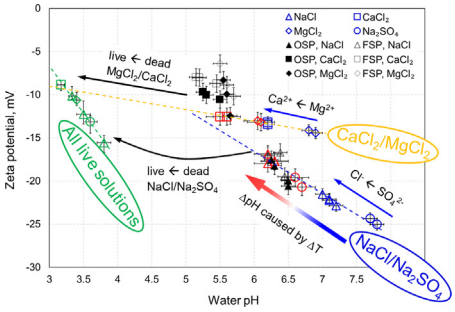

ARTICLE INFO

Article history:
Received 13 August 2021
Revised 13 September 2021
Accepted 14 September 2021
Available online 17 September 2021

Keywords:
Zeta potential
Sandstone
Elevated temperature
High pressure
Supercritical CO_2 conditions
Carbonated aqueous solution
Streaming potential method

ABSTRACT

Despite the broad range of interest and applications, controls on the electric surface charge and the zeta potential of silica in contact with aqueous solutions saturated with dissolved CO_2 at conditions relevant to natural systems, remains unreported. There have been no published zeta potential measurements conducted in such systems at equilibrium, hence the effect of composition, pH, temperature and pressure remains unknown.

We describe a novel methodology developed for the streaming potential measurements under these conditions, and report zeta potential values for the first time obtained with Fontainebleau sandstone core sample saturated with carbonated NaCl, Na_2SO_4, $CaCl_2$ and $MgCl_2$ solutions under equilibrium conditions at pressures up to 10 MPa and temperatures up to 40 °C.

The results demonstrate that pH of solutions is the only control on the zeta potential, while temperature, CO_2 pressure and salt type affect pH values. We report three empirical relationships that describe the pH dependence of the zeta potential for: i) dead (partial CO_2 pressure of $10^{-3.44}$ atm) $NaCl/Na_2SO_4$, ii) dead $CaCl_2/MgCl_2$ solutions, and iii) for all live (fully saturated with dissolved CO_2) solutions. The proposed new relationships provide essential insights into interfacial electrochemical properties of silica-water systems at conditions relevant to CO_2 geological storage.

* Corresponding author.
E-mail addresses: jan.vinogradov@abdn.ac.uk, janvin71@gmail.com (J. Vinogradov).

https://doi.org/10.1016/j.jcis.2021.09.076
0021-9797/

1. Introduction

Quartz is a common mineral comprising 12% of the Earth's crust [1]. Quartz is also the constituent mineral of sandstone formations, and it can be found in many subsurface settings including aquifers (e.g., [2,3]), hydrocarbon reservoirs (e.g., [4,5]) and geothermal sources (e.g., [6,7]). To characterize the subsurface flows in such settings, a variety of electrical geophysical methods are available including electrical resistivity tomography (e.g., [8,9]), electro-seismic (injecting electric current and measuring the resulting seismic energy; e.g., [10,11]), seismo-electric (generating a seismic wave and measuring the resulting electric field; e.g., [11,12]) and self-potential (SP) (voltage that arises in response to existing gradients in pressure, concentration or temperature; e.g., [13,14]) measurement. The SP has been shown to be an efficient method to characterize single- and multi-phase flows in the subsurface, especially in sandstone reservoirs (e.g., [15,16]). Moreover, the SP method can characterize permeability heterogeneities (e.g., fractures, faults, and variable permeability zones [17,18]).

The SP method relies on electrochemical processes that arise in response to the establishment of an electrical double layer (EDL) at the rock-water interface; this can be characterized by the zeta potential (e.g., [19,20]). The zeta potential also plays an important role in determining the wettability (e.g., [21]); while the wetting state controls the pore occupancy of aqueous solutions (hereafter referred to as water for simplicity) and non-aqueous phase fluids (NAPF) in multi-phase systems, and thus strongly influences fluid saturations and flow patterns, e.g. in CO_2 geological storage (CGS) [22], hydrocarbon recovery [23], or H_2 geo-storage [24].

There are three principal forces (namely van der Waals, structural and electrostatic forces [25]) that act between rock-water and NAPF-water interfaces; these forces determine the disjoining pressure, which in turn controls the wetting state. Structural forces are always repulsive, thus implying a positive (repulsive) contribution to the disjoining pressure [25,26], while van der Waals forces depend on properties of all constituent phases (refractive index, dielectric constant and absorption frequency), and these forces can be characterized by the Hamaker theory, resulting in either positive or negative [25,27,28] to the disjoining pressure. Electrostatic forces can also be positive or negative [25,29] depending on rock mineralogy, water pH, ionic strength and chemical composition. The magnitude and polarity of the electrostatic forces depend on the interfacial zeta potentials, which can vary substantially [26], therefore these forces play a key role in controlling the wettability.

In order to accurately characterize the wettability, the measured experimental data of zeta potential of rock-water and NAPF-water interfaces is essential. There are two common methods available for measuring zeta potential; namely the electrophoretic mobility and streaming potential. The electrophoretic mobility method (EPM) relies on the motion of the dispersed phase (either rock or NAPF) relative to the continuous stationary water phase under the influence of an applied electric field [30]. In contrast, the streaming potential method (SPM) is based on the flow of water through a stationary porous medium, which may also contain NAPF, under the influence of a pressure gradient [20,30]. The benefits of using EPM include a relative ease of use commercially available instruments. However, the measurement conditions are far from representative of deep subsurface settings for several reasons. Firstly, EPM cannot currently be used under high pressure and elevated temperature conditions, or with high ionic strength electrolytes (>1M; M = mol•L^{-1}), the conditions that are typical for deep rock formations [26]. Secondly, EPM requires either a powdered mineral sample or emulsified NAPF dispersed in water and therefore, it cannot capture the true complex pore space topology [26]. Finally, EPM cannot take into account a third phase, which is needed for multi-phase flow (e.g., water and gas) [31]. In contrast, SPM can be used on intact sandstone samples (e.g., [32,33]), at elevated temperature (e.g., [16]), using low-to-high salinity electrolytes of simple and complex composition (e.g., [34]) and also on multi-phase systems containing water, NAPF and minerals at the same time (e.g., [35,36]). However, conducting SPM experiments is challenging and time consuming. In addition, to the best of our knowledge, thus far there has been no published study that reported either EPM or SPM zeta potential measurements under high pore pressure and elevated temperature conditions, typical for deep subsurface settings. Acquisition of the high pore pressure and elevated temperature data is particularly important as gas under these conditions (e.g., CO_2 during carbon dioxide sequestration or CO_2 injection for improved oil recovery) dissolves in water to a higher degree and alters the ionic composition, reduces pH, so that the resulting aqueous solution becomes the so-called carbonated water (C_water). Such changes in water chemistry will have an impact on the C_water-rock and C_water-NAPF zeta potentials and will ultimately affect the wettability and dynamics of flow of each fluid. Note, that the term C_water used in this study corresponds to any aqueous solution with non-zero concentration of dissolved CO_2.

Several attempts have been made to measure the zeta potential in CO_2 containing systems. A recent study published by Kim and Kwak [37] reported the zeta potential of CO_2-water interfaces using EPM. The experiments were conducted by bubbling CO_2 gas through 0.01 M NaCl solution. The zeta potential was reported to be negative, but the experiments were conducted at atmospheric pressure and unreported temperature. Another study by Moore et al. [38] reported measurements of the zeta potential using SPM in Berea sandstone samples saturated with tap water and liquid CO_2. The experiments were conducted at a maximum pressure of 6.5 MPa and temperature of 20 °C, so that the latter value is not consistent with the expected temperature of 38 °C normally found at the depth that corresponds to 6.5 MPa [39]. The single-phase zeta potential was measured in rock sample fully saturated with water, which was not carbonated prior to the experiments, i.e., the amount of dissolved CO_2 corresponded to the atmospheric level. The experiment was repeated with water and immiscible liquid CO_2 and the effective (i.e., multi-phase) zeta potential was found to be negative and approximately ten-fold smaller in magnitude compared with the single-phase zeta potential. However, Moore et al. [38] did not report single-phase zeta potential measurements conducted with C_water under the same experimental conditions, hence the contribution of the zeta potential at the interface between water and immiscible liquid CO_2 could not be quantified. Moreover, Moore et al. [38] did not report the equilibrium pH of water during the experiments, to indicate whether chemical equilibrium between the mineral, water and liquid CO_2 was established. Since pH is known to have a strong effect on the silica-water zeta potential [16,40], uncertainty exists in relation to Moore et al.'s [38] reported multi-phase zeta potential results. Furthermore, to the best of our knowledge, no experimental zeta potential data for C_water-rock or C_ water-immiscible CO_2 interfaces under high pressure and elevated temperature conditions has been reported (which are typical for deep subsurface formations). Note that in CGS, CO_2 is stored below a depth of 800 m, so that the CO_2 exists in a dense supercritical phase [41,42] which correspond to the critical point of CO_2 is 7.38 MPa and 31.1 °C).

In the absence of such measured zeta potential data, several models have been proposed with which the wettability of sandstones can be predicted. For instance, Tokunaga [43] and Kim et al. [44] reported an analytical model of water film stability,

based on DLVO (Derjaguin, Landau, Verwey, Overbeek) theory; the model was used to simulate CO_2 geological storage (CGS) conditions in sandstone reservoirs. The model required knowledge of the electrostatic interactions between silica-water and CO_2-water interfaces, to calculate the corresponding contribution to the disjoining pressure, and the model was implemented using compression approximation [45]. Tokunaga [43] and Kim et al. [44] assumed that the zeta potential of the silica-water interface was −25 mV for 0.01 M ionic strength solution, and −5 mV for 2 M ionic strength. Both, Tokunaga [43] and Kim et al. [44] assumed a zero zeta potential at the CO_2-water interface. However, neither of the assumed values was validated due to a lack of experimental data under true CGS conditions. Moreover, when the CO_2 dissolves in water at high pressure, and the pH of C_water becomes substantially lower [46,47], the zeta potential of C_water-silica interfaces should become vanishingly small [48]. This, however, is inconsistent with the assumed values by Tokunaga [43] and Kim et al. [44], thus their wettability estimates are also doubtful.

Therefore, the main aim of this study is to develop an experimental methodology and for the first time measure the streaming potentials in intact sandstone samples under high pressure and elevated temperature, using C_water, to improve our understanding of the electrochemical processes that take place at silica-water interfaces. The outcomes of this study will, among other applications, better inform CGS, hydrocarbon recovery and geothermal projects. This work also provides fundamental petrophysical data essential for a broad range of Earth sciences.

2. Materials and methods

2.1. Materials

A cylindrical Fontainebleau sandstone sample was used in this study. Petrophysical properties of the sample listed in Table 1 suggest partial cementation, in line with the values of porosity and formation factor [32], which was important for repeated saturation. Prior to conducting the streaming potential measurements, the sample was thoroughly cleaned following the procedure reported by Alroudhan et al. [31]. We used synthetic single-salt solutions made with reagent-grade NaCl, $CaCl_2{\cdot}2H_2O$, $MgCl_2{\cdot}6H_2O$, and Na_2SO_4 (Sigma Aldrich, Australia) dissolved in deionized (DI) water. The DI water (electrical resistivity 15 MΩ·cm −18 MΩ·cm) was supplied by a filtering system from Ibis Technology (Ascot, Australia). The ionic strength of all four solutions was kept constant at 0.05 M during preparation under laboratory (ambient) pressure and 23 °C temperature. All laboratory experiments were conducted using two types of aqueous solutions: 'dead' and 'live' water. The dead water was a synthetic aqueous solution fully equilibrated with atmospheric CO_2 (which corresponds to partial CO_2 pressure of $10^{-3.44}$ atm and to a dissolved CO_2 concentration of 1.487×10^{-5} M [51]). The CO_2 content of the dead water remained unchanged throughout the experiment. On the other hand, to prepare the live water we used a salt solution prepared under ambient pressure and temperature, which subsequently was brought in contact with pure CO_2 (supplied by Coregas, Australia, with the mole fraction $\geq$ 0.99) in a mixing reactor [52]. The system was pressured and heated to target experimental pressure and temperature. Allowing CO_2 and water to mix for a long period of time in the reactor (no less than 3 h); while measuring the volume of the CO_2 cap until it stabilized under constant pressure, the thermodynamic equilibrium between water and CO_2 was established. The target pressure and temperature that corresponded to the live water equilibrium was maintained throughout each experiment.

Prior to carrying out the streaming potential measurements with dead water, the saturated rock sample was placed in a core holder, and the entire system was sealed from atmosphere. The detailed experimental protocol of the streaming potential measurement using both dead and live water is provided in subsequent sections.

Table 1
Petrophysical properties of the Fontainebleau sandstone sample used in this study. Mineralogy of the sample was taken from [34,49,50]. Sample porosity was measured by gas (N_2) expansion using AP-608 Automated Permeameter and Porosimeter (Coretest System Inc, USA). The formation factor was obtained with five dead NaCl solutions with ionic strength between 0.05 M and 1 M. The liquid permeability was calculated using Darcy's Law from the slope of linear regression of the flow rate against the pressure difference during the streaming potential measurements using at least four different flow rates with confirmed high quality of regression ($R^2 \geq 0.98$).

Sample	Fontainebleau sandstone
Mineralogy	>99 wt% quartz
Porosity	9.0 ± 1.0%
Liquid Permeability	70 ± 5 mD ($6.91 \times 10^{-14} \pm 4.93 \times 10^{-15}$ m^2)
Dimensions	Length = 0.0783 m, Diameter = 0.0382 m
Formation Factor, *F*	58 ± 2

2.2. Measurements of pH and, water and saturated rock electrical conductivity

The dead water experiments were conducted at pore pressures up to 10 MPa and temperatures up to 40 °C. Since the concentration of dissolved CO_2 remained constant at atmospheric level during the dead water experiments (in the closed system), effluent water samples were regularly collected and pH values and electrical conductivities were measured outside the system using a FiveGo pH meter (Mettler Toledo, accuracy of 0.01 pH units) and a Jenway 4520 conductivity meter (Cole-Palmer, 0.5% accuracy), respectively.

The live water experiments were carried out over the same pressure ranges (up to 10 MPa backpressure) and temperatures of 40 °C. Live water pH values were measured using an in-line high-pressure pH meter (Corr Instruments, LLC). Both pH meters, as well as the conductivity meter were regularly calibrated using standard solutions and manufacturer's recommended procedure.

The chemical equilibrium between the rock sample and all aqueous solutions was assured using pH and water electrical conductivity measurements on a regular basis as detailed by Vinogradov and Jackson [16]. Therefore, the measured pH values and water conductivities reported here represent the equilibrium values (for a given solution, pressure and temperature). Dead and live water properties are provided in Table 2.

The saturated rock conductivity (σ_{rw}) was measured in-situ using a pair of internal electrodes and following the procedure of Vinogradov et al. [34]. The intrinsic formation factor (F) was obtained prior to carrying out the streaming potential measurements using NaCl solutions between 0.05 M and 1 M, and following the protocol of Vinogradov et al. [34].

2.3. Experimental setup

The streaming potential measurements were conducted in a high pressure-high temperature (HPHT) coreflooding apparatus (schematically shown in Fig. 1). The coreflooding apparatus was placed inside an oven with controlled temperature (accuracy of ±1 °C). For the dead water experiments, the branch of the experimental apparatus comprising units #10 - #12 (Fig. 1), used for preparing live water, was disconnected from the rest of the setup.

The pressure difference across the core sample was measured continuously with a high precision Keller-Druck pressure transducers (0.1% accuracy). Furthermore, the voltage across the sample was recorded with a NI 9207 voltmeter with high internal impedance (>1 GΩ) and 0.52% accuracy. Two high precision syringe

Table 2
Dead and live water properties for all tested experimental conditions, where P is the pore pressure, T is the experimental temperature, σ_w is the elctrical conductivity of tested solution. pH values reported for all dead water experiments correspond to partial CO_2 pressure of $10^{-3.44}$ atm. The ionic strength of all solution was kept constant at 0.05 M. The reported uncertainties in the table are based on both the instrument accruracy and measurement repeatability. The total uncertainty in σ_w was ± 0.01 S/m in all experiments.

Solution	P, MPa	T, °C	Solution type	pH value	σ_w, S/m
NaCl	0.2	23	Dead water	7.10 ± 0.10	0.55
	4.5	23	Dead water	7.00 ± 0.10	0.55
	7.5	23	Dead water	7.10 ± 0.10	0.56
	10.0	23	Dead water	7.20 ± 0.10	0.55
	0.2	40	Dead water	6.30 ± 0.20	0.61
	4.5	40	Dead water	6.30 ± 0.20	0.60
	7.5	40	Dead water	6.20 ± 0.20	0.61
	10	40	Dead water	6.20 ± 0.20	0.60
	4.5	40	Live water	3.80 ± 0.10	0.65
	7.5	40	Live water	3.50 ± 0.10	0.64
	10.0	40	Live water	3.33 ± 0.05	0.55
$CaCl_2$	0.2	23	Dead water	6.20 ± 0.10	0.34
	7.5	23	Dead water	6.20 ± 0.10	0.34
	0.2	40	Dead water	5.60 ± 0.20	0.46
	7.5	40	Dead water	5.50 ± 0.20	0.46
	7.5	40	Live water	3.17 ± 0.05	0.54
$MgCl_2$	0.2	23	Dead water	6.90 ± 0.10	0.37
	7.5	23	Dead water	6.80 ± 0.10	0.37
	0.2	40	Dead water	6.05 ± 0.20	0.51
	7.5	40	Dead water	6.10 ± 0.20	0.51
	7.5	40	Live water	3.40 ± 0.05	0.50
Na_2SO_4	0.2	23	Dead water	7.80 ± 0.10	0.36
	7.5	23	Dead water	7.70 ± 0.10	0.36
	0.2	40	Dead water	6.70 ± 0.20	0.48
	7.5	40	Dead water	6.70 ± 0.20	0.48
	7.5	40	Live water	3.60 ± 0.10	0.59

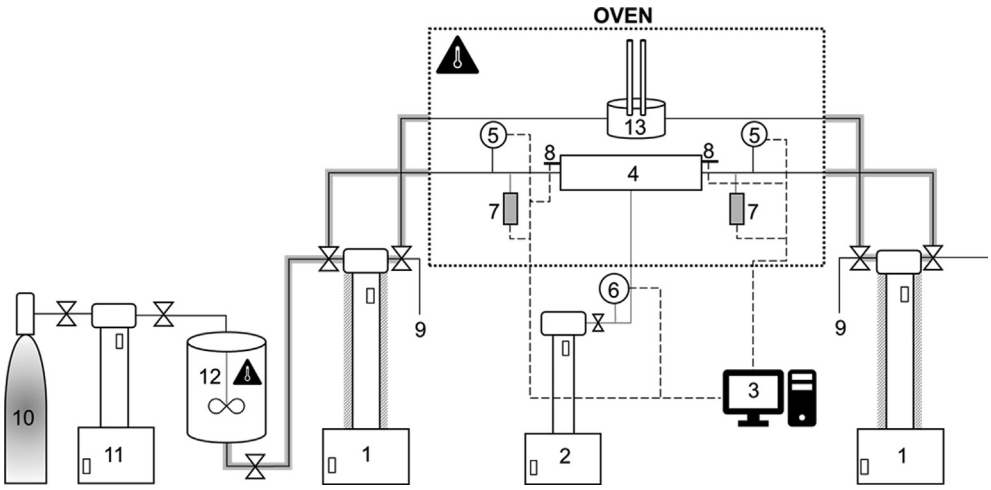

Fig. 1. The experimental apparatus used in streaming potential measurements. The solid grey lines represent flowlines and the dashed grey lines represent electrical connections. (#1) heated 500D Hastelloy ISCO pumps to the left and to the right of the core holder; (#2) 500D is a stainless steel ISCO pump used to induce the confining pressure around the rock sample; (#3) data acquisition system; (#4) is the HPHT coreflooding cell (core holder); (#5) two high precision pressure transducers; (#6) high precision pressure transducer used to monitor the confining pressure; (#7) external electrodes to the left and to the right of the core holder; (#8) internal electrodes to the left and to the right of the core holder; (#9) are sampling tubes to the left and to the right of the core holder; (#10) CO_2 cylinder; (#11) 260D Stainless steel ISCO pump used for pumping CO_2 into the mixing reactor; (#12) heated Parr mixing reactor; (#13) high pressure in-line pH meter.

pumps (#1 in Fig. 1; 500D Hastelloy ISCO) were used as injector and receiver to induce water flow in either direction through the sample. The pump used as injector was set to deliver water at a constant flow rate while the receiving pump on the opposite side was set at a constant receiving pressure (i.e., maintaining a constant back pressure during the experiment). During all coreflooding experiments, the difference between the confining pressure and the pore pressure was kept constant at approximately 3 MPa. The maximum difference between the injection and the outlet pressure that corresponds to the highest tested flow rate was 0.14 MPa. Constant target temperature was maintained during the experiments by heating cylinders of both pumps with an embedded water jacket and insulating all flowlines outside the oven to prevent heat losses. Upon completion of each streaming potential experiment, the saturated rock conductivity was measured using the internal electrodes (#8) connected to a BK Precision 891 LCR meter (0.05% accuracy), by sweeping the applied alternate voltage frequency between 20 Hz and 300 KHz.

2.4. Streaming potential measurements in rock samples saturated with dead water

The streaming potential method was used to obtain the zeta potential of the rock-water interface. The method relies on the

assumption that at steady state, the streaming current is balanced by the conduction current during one-directional flow of water through the porous medium, consistent with our core flooding experiments where stable pressure and voltage were established across the rock sample. To achieve such conditions, the paired-stabilized (PS) method described in Vinogradov and Jackson [36] was implemented to measure the streaming potential coupling coefficient (C_{SP}). Employing the PS method also allowed us to eliminate any asymmetry in the electrode potential as detailed in [34]. C_{SP} was interpreted from the slope of linear regression of stabilized (normalized) voltage (see Equation 7a in Vinogradov et al. [34]) as a function of stabilized pressure difference (normalized ΔP; see Equation 7b in Vinogradov et al. [34]). The zeta potential (ζ) was then calculated via the modified Helmholtz-Smoluchowski equation (which accounts for the surface electrical conductivity [20,53,54]):

$$C_{SP} = \frac{\Delta V}{\Delta P} = \frac{\varepsilon \zeta}{\mu \sigma_{rw} F} \quad (1)$$

where ΔV is the stabilised voltage in [V], ΔP is stabilised pressure [Pa], ε is the water permittivity in [F·m^{-1}], μ is the water dynamic viscosity in [Pa·s], σ_{rw} is the electrical conductivity of the saturated rock sample in [S·m^{-1}] and F is the intrinsic formation factor, which was found to be constant for all tested solutions implying negligibly small surface conductivity even at the lowest tested ionic strengths (refer to S1 is supplementary material). Note, that since $F = \frac{\sigma_w}{\sigma_{rw}} = 58$ was constant for all tested solutions, Eq. (1) reduces to the classical Helmholtz-Smoluchowski equation and water conductivity can also be used to compute the zeta potential. We calculated ε and μ to account for the temperature and ionic strength using the correlations provided in Saunders et al. [55].

2.5. Streaming potential measurements in rock samples saturated with live water

The live water experiments required several modifications to the apparatus and the experimental protocol due to the corrosive nature of the live water. The new procedure in detailed below.

During the rock sample preparation step, an additional layer of thin polytetrafluoroethylene (PTFE) tape was wrapped around the rock sample, and a PTFE heat shrinkable sleeve was placed around the PTFE taped sample. The entire assembly was then placed inside a Viton sleeve, which was thus isolated from the corrosive pore fluid. The sample inside the Viton sleeve was mounted into the core holder (#4) and pressurized with dead water as a confining fluid (note, that Viton is not compatible with acids).

For preparing live water, 500 mL dead water were placed in the mixing reactor (#12), and the reactor was closed with a small air cap left at the top of the dead water. The reactor was heated overnight by circulating hot water in its water jacket to the target 40 °C at atmospheric pressure so that the experimental temperature was established.

Fluid equilibration started with the delivery of CO_2 at 4 MPa from the CO_2 cylinder (#10) to the pre-emptied high precision syringe pump (#11). Subsequently, the CO_2 in the pump was pressurized to the target pore pressure (4,5 MPa, 7.5 MPa or 10 MPa), and pumped through flowlines into the mixing reactor using constant pressure delivery mode. The volume of the CO_2 remaining in the pump (#11) was constantly monitored, and the pressure in the reactor (#12) was equilibrated with that of the pump (#11) using the constant pressure delivery mode, and the gas entrainment stirrer inside the reactor was activated to rigorously mix the liquid phase (water) and the CO_2 cap at the top (thus accelerating the equilibration [52]). Equilibrium between the water and CO_2 phases was assumed to have been established when the volume of CO_2 inside the pump ceased to decrease and remained constant for at least 3 h thus indicating that no additional CO_2 dissolved in water. At this stage, we assumed the water was fully saturated with CO_2 and it was transferred from the reactor to the injection pump (#1, to the left of the core holder in Fig. 1) for the experiments.

Due to technical limitations of the injection pump (#1), all of the live water in the reactor (#12) was transferred to the pump (#1 to left of the core holder in Fig. 1) containing approximately 5 mL of dead water. Moreover, the setup's dead volumes (valves, tubing), the pore space of the rock sample, and the receiving pump (#1 to the right of the core holder in Fig. 1) also contained pressured (to the same pressure as that in the injection pump) dead water. In total, 400 mL of fully CO_2 saturated live water was mixed with approximately 30 mL of dead water remaining in the system, thus disturbing the chemical and thermodynamic equilibrium. Therefore, to re-equilibrate the system, flow of the mixed solution was induced from left to right and back again. The procedure that usually lasted for at least 2 days was repeated several times while regularly measuring the pH, rock permeability, electrical conductivity of the sample and C_{SP}, until all properties stabilized at constant values (within 2% tolerance). The confirmed stability of electrical conductivity of the saturated rock sample and its permeability throughout the equilibration period also indicated there was no measurable dissolution or precipitation of minerals.

The streaming potential measurements then commenced and were completed using at least 4 different flow rates following the recommended PS procedure [36]. To measure the voltage across the rock sample in live water experiments only the internal electrodes (#8) were used (details on design and materials used for the internal electrodes are provided in [34]) due to their higher stability relative to that of the external electrodes. The zeta potential was interpreted from the measured C_{SP} using Eq. (1), for which the updated values of σ_{rw}, ε and μ of live water were required (F remained constant in all reported single-phase experiments).

The live water saturated rock conductivity (σ_{rw}) was measured in each experiment. Live water electrical conductivity (σ_w) was calculated by multiplying the intrinsic formation factor (assumed to be constant and equal to that measured with the corresponding dead water) by the live water saturated rock conductivity and all values are reported in Table 2. The live water ionic strength (salinity) was determined using σ_w (refer to section 2.6 in Vinogradov et al. [34]), and the salinity was then used to adjust the permittivity of live water (ε) using the approach described in Saunders et al. [55].

The viscosity of the live water (μ_{lw}) at given pressure and temperature was then calculated via the approach proposed by Islam and Carlson [56]:

$$\mu_{lw} = \mu_s \times \left(1 + 4.65 x_{CO_2}^{1.0134}\right) \quad (2)$$

where μ_s in [Pa·s] is the viscosity of dead water as a function of pressure and temperature, and xCO_2 is the mass fraction of dissolved CO_2 at experimental conditions. Due to the lack of published measurements of μ_s for all tested salt types and temperatures of our dead solutions, we adopted the approach of Saunders et al. [55] to infer the dead water viscosity from the measured electrical conductivity. The calculated values of μ_s for our dead solutions were compared against available published data (for the same salts at concentrations and temperatures consistent with our experimental conditions), and the discrepancy was found to be less than 2% thus confirming the appropriateness of the approach.

The mass fraction of dissolved CO_2 (xCO_2) was evaluated using the model of Zhao et al. [57,58] and validated for 0.05 M NaCl live water against the experimental values reported by Islam and Carlson [56] for 40 °C and 7.5 MPa, and was found to be identical within 1% discrepancy.

The exponent in Eq. (2) was assumed to be constant for all types of live water investigated here, since it only defines how the solubility of CO_2 depends on the salt type, and the solubility was reported to be nearly identical for all tested salts at ionic strength of 0.05 M (e.g., [59]).

3. Results and discussion

3.1. Streaming potential coupling coefficient measurements

Typical results of PS experiments for select experimental conditions are shown in Fig. 2. The noise level of the stabilized voltage measured for live water (Fig. 2c) was considerably higher than for dead water (Fig. 2a). Moreover, the static voltage (i.e., the voltage that corresponds to no-flow conditions and zero pressure difference across the sample) measured for live water did not always return to the exact initial value (as prior to the core flooding experiment), thus contributing to additional error in the streaming potential coupling coefficient and the corresponding zeta potential.

Experimental repeatability at a given flow rate with live water was also poorer when compared with dead water (compare the scatter for a given pressure difference in Fig. 2b and d). The values of all measured streaming potential coupling coefficients inclusive of all experimental uncertainties (obtained from the variation in the slope of the linear regression within the error bars that account for the noise level and repeatability, as shown in Fig. 2b and 2d) are summarized in Table 3.

3.2. Dead water zeta potential

Zeta potentials for dead water remained negative for all tested conditions. Moreover, for any given temperature and salt type, the zeta potential was independent of the pore pressure (Fig. 3a). Dead water equilibrium pH values were also independent of pore pressure for any given salt type (Fig. 3b), which implied that the amount of dissolved CO_2 remained constant during the experiments. However, pH decreased with increasing temperature, consistent with previously reported studies [16,40,60,61].

The largest in magnitude zeta potential was obtained with Na_2SO_4, and it became progressively smaller in magnitude when using NaCl, $MgCl_2$ and $CaCl_2$, ($|\zeta_{Na_2SO_4}| > |\zeta_{NaCl}| > |\zeta_{MgCl_2}| > |\zeta_{CaCl_2}|$). A difference of less than 1 mV between the zeta potentials of $MgCl_2$ and $CaCl_2$ was observed for both salts at both temperatures of 23 °C and 40 °C. Although this difference was small, it was comparable to the difference of 2 mV reported by Vinogradov et al. [40] for the same salt types. The measured pH of solutions in contact with the sample became smaller with the transition from Na_2SO_4 to NaCl, followed by $MgCl_2$ and $CaCl_2$ ($pH_{Na_2SO_4} > pH_{NaCl} > pH_{MgCl_2} > pH_{CaCl_2}$), qualitatively consistent with previously published studies [40,62].

To quantify the effect of salt type and temperature, zeta potential and water pH were plotted versus temperature (Fig. 4). The zeta potential became more positive with increasing temperature, while water pH decreased with increasing temperature, consistent with previously published results [16,40]. The highest rate of increase in the zeta potential with temperature was observed for NaCl (a change of +4.3 mV when transitioning from 23 °C to 40 °C). An increase in zeta potential (+4.3 mV) was also observed for Na_2SO_4 when temperature increased from 23 °C to 40 °C. In contrast, zeta potential increased with increasing temperature by 1.0 mV for both, $CaCl_2$ and $MgCl_2$, when temperature increased from 23 °C to 40 °C. Therefore, a weaker temperature dependence of the zeta potential was observed for $CaCl_2$ and $MgCl_2$, again consistent with Vinogradov et al. [40].

However, the rate of pH change with temperature was higher when compared to Vinogradov et al. [40]. Moreover, the pH values

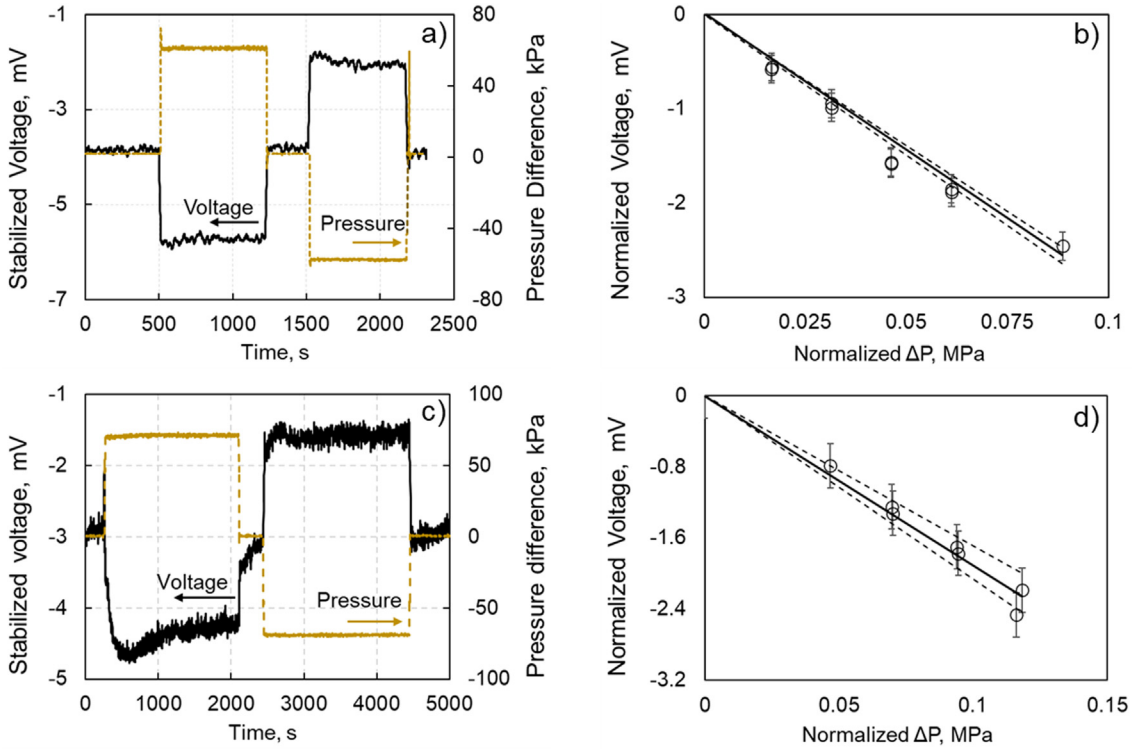

Fig. 2. Typical results of paired stabilized (PS) experiments (a, c) and the streaming potential coupling coefficient represented by the linear slope of the stabilized voltage, ΔV, plotted against the stabilized pressure difference, ΔP (b, d). (a) dead NaCl solution pumped at a constant rate of 4 mL/min, temperature of 23 °C and pore pressure of 7.5 MPa); (b) C_{SP} interpreted from the data of (a); (c) typical data of PS experiment carried out with live NaCl solution at constant rate of 6 mL/min, temperature of 40 °C, pressure of 7.5 MPa; d) C_{SP} interpreted from the data of (c). Dashed lines represent possible variation of C_{SP} within the total experimental uncertainty denoted by the error bars.

Table 3
Streaming potential coupling coefficient (C_{SP}) measured for all tested experimental conditions. The ionic strength of all solution was kept constant at 0.05 M. The reported uncertainties in the table are based on both noise level and repeatability, both of which results in linear regressions slope variation as shown in Fig. 2b and d.

Water	Pressure, MPa	Temperature, °C	Condition	C_{SP}, mV/MPa
NaCl	0.2	23	Dead water	-29.9 ± 0.07
	4.5	23	Dead water	-29.9 ± 0.07
	7.5	23	Dead water	-29.9 ± 0.07
	10.0	23	Dead water	-30.7 ± 0.07
	0.2	40	Dead water	-28.8 ± 0.10
	4.5	40	Dead water	-28.3 ± 0.10
	7.5	40	Dead water	-28.5 ± 0.10
	10.0	40	Dead water	-28.3 ± 0.10
	4.5	40	Live water	$-23.6^{+1.20}_{-1.30}$
	7.5	40	Live water	$-19.0^{+2.00}_{-1.60}$
	10.0	40	Live water	$-18.1^{+1.80}_{-0.70}$
$CaCl_2$	0.2	23	Dead water	-26.5 ± 0.07
	7.5	23	Dead water	-26.9 ± 0.07
	0.2	40	Dead water	-25.3 ± 0.10
	7.5	40	Dead water	-25.4 ± 0.10
	7.5	40	Live water	$-17.6^{+0.90}_{-1.20}$
$MgCl_2$	0.2	23	Dead water	-28.0 ± 0.07
	7.5	23	Dead water	-28.4 ± 0.07
	0.2	40	Dead water	-27.4 ± 0.07
	7.5	40	Dead water	-27.3 ± 0.07
	7.5	40	Live water	$-17.8^{+1.40}_{-1.00}$
Na_2SO_4	0.2	23	Dead water	-56.4 ± 0.12
	7.5	23	Dead water	-55.6 ± 0.12
	0.2	40	Dead water	-44.8 ± 0.20
	7.5	40	Dead water	-43.1 ± 0.20
	7.5	40	Live water	$-24.1^{+1.20}_{-2.20}$

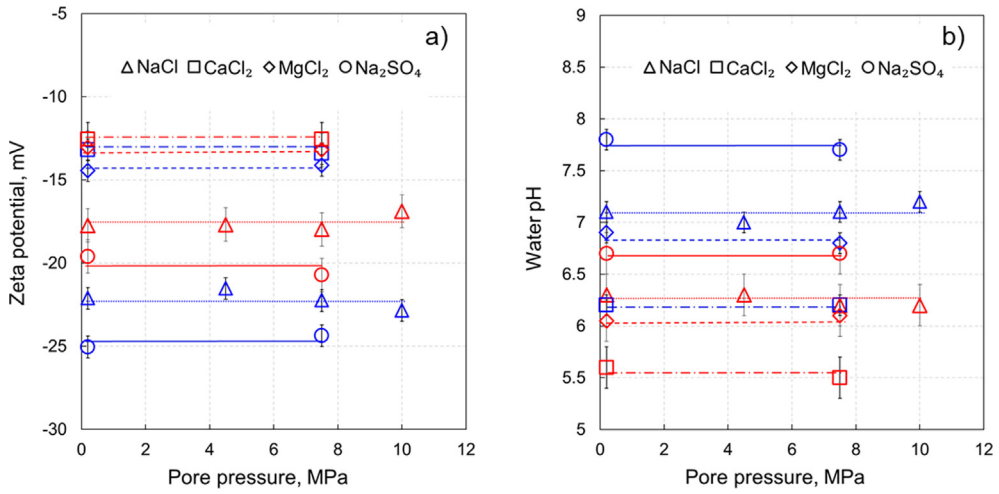

Fig. 3. Zeta potential a) and pH values b) as a function of pore pressure for all dead water experiments. Blue symbols denote experiments conducted at 23 °C; red symbols denote experiments conducted at 40 °C. (For interpretation of the references to color in this figure legend, the reader is referred to the web version of this article.)

measured in our experiments were generally larger than those in Vinogradov et al. [40] for the same salt type at any given temperature. The ionic strength used by Vinogradov et al. [40] was 0.015 M, which is more than three-fold lower than that tested in this study, hence their zeta potentials at lower salinity were expected to be larger in magnitude compared to ours. Since the zeta potentials reported by Vinogradov et al. [40] were smaller in magnitude compared with our results, we believe that their pH values were correct, although different from ours, and had stronger effect on the zeta potential than salinity.

Our results suggest that temperature and salt type affect the pH, which in turn affects the magnitude of the zeta potential of sandstones saturated with dead water (Fig. 5). Based on the results for dead water we propose two distinct linear correlations:

$$\zeta_M[mV] = -4.86 \times pH + 12.57; R^2 = 0.976 \quad (3)$$

$$\zeta_D[mV] = -1.35 \times pH - 4.96; R^2 = 0.973 \quad (4)$$

where ζ_M and ζ_D denote the zeta potential for water containing monovalent (Na^+) or divalent (Ca^{2+} and/or Mg^{2+}) cations, respectively. Regardless of anion type (Cl^- or SO_4^{2-}) all experimental points for Na^+ containing solutions align on the same trendline, and so do the points for all $CaCl_2$ and $MgCl_2$ experiments regardless of the cation type (Fig. 5).

The trend obtained for Na^+ solutions (Eq. (3)) is identical to that reported for zeta potentials of sandpacks [40]. However, as seen in Fig. 5 the zeta potentials at 23 °C measured in this work (blue triangles) were more negative compared with values of Vinogradov et al. [40] and corresponded to higher pH values. The values that correspond to 40 °C were consistent with those reported by Vinogradov et al. [40] thus implying stronger temperature effect on both pH and zeta potentials.

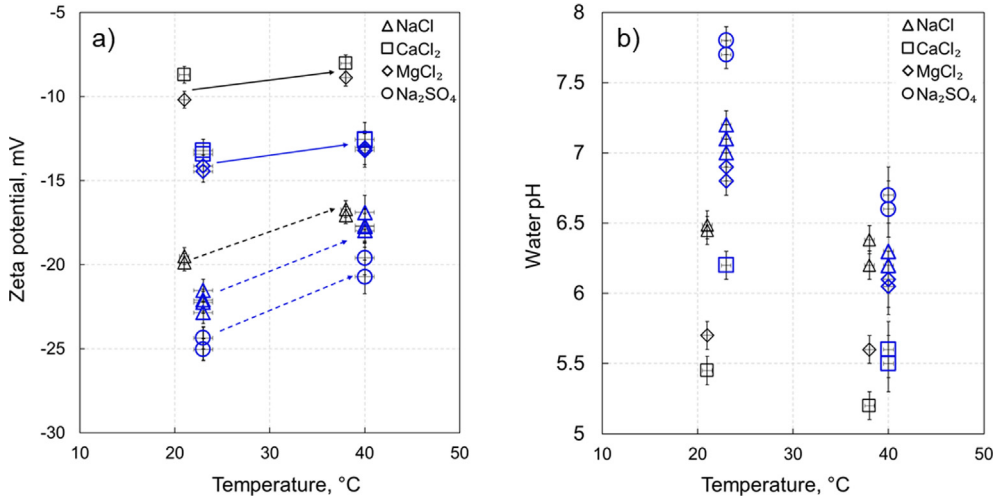

Fig. 4. Zeta potential a) and pH values b) as a function of temperature for all tested dead water experiments. The data for NaCl, $CaCl_2$, $MgCl_2$ and Na_2SO_4 obtained in this work are shown in blue. Also shown for comparison are the data in black obtained with Fontainebleau sandpacks saturated with 0.015 M solution NaCl, $CaCl_2$ and $MgCl_2$ reported by Vinogradov et al. [40]. (For interpretation of the references to color in this figure legend, the reader is referred to the web version of this article.)

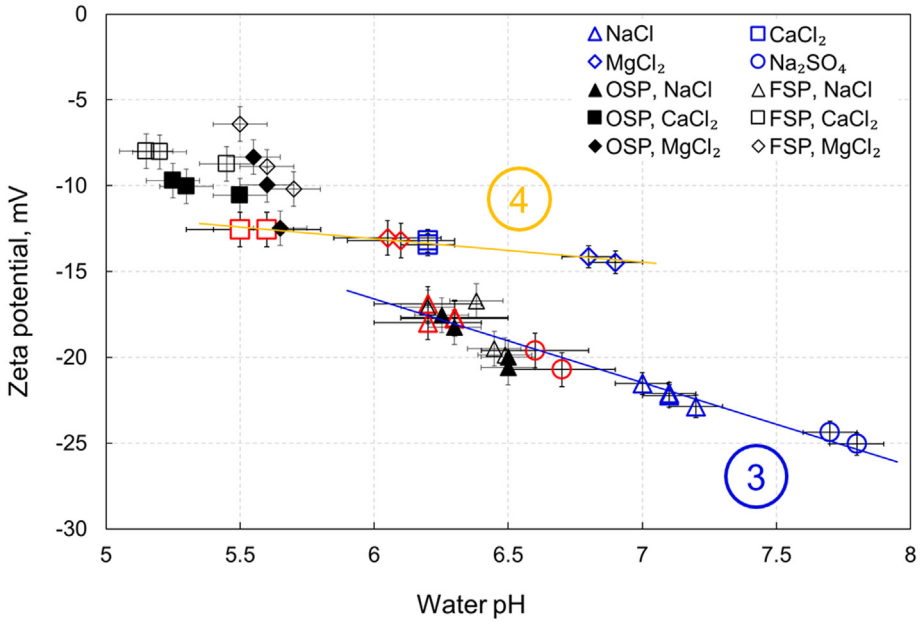

Fig. 5. Zeta potential as a function of dead water pH for different salt types. Our data are shown in colored symbols; literature data are shown in black [40] and corresponds to Ottawa (OSP) and Fontainebleau (FSP) sandpacks (both > 99 wt% quartz content) saturated with 0.015 M dead water. Blue symbols correspond to 23 °C, red symbols correspond to 40 °C. The blue trendline indicates the linear relationship between the zeta potential of Na^+ containing salts (NaCl, Na_2SO_4) and pH (Eq. (3)). The yellow trendline indicates the linear correlation between zeta potential and pH of dead $CaCl_2$ and $MgCl_2$ solutions (Eq. (4)). (For interpretation of the references to color in this figure legend, the reader is referred to the web version of this article.)

In contrast, the trend for divalent cations (Eq. (4)) had a flatter slope, compared with that of Eq. (3). Such flattening of the slope is consistent with the pH dependence of $CaCl_2$ solution relative to that of NaCl proposed by Vinogradov et al. [40]. Overall, however, all our ζ_D were more negative than those reported by Vinogradov et al. [40], except for the value at pH = 5.7.

The effect of temperature on pH of divalent solutions ($CaCl_2$, $MgCl_2$), denoted by the shift from blue to red symbols in Fig. 5, was substantially more pronounced in this work compared to Vinogradov, et al. [40]. Moreover, Vinogradov et al. [40] also suggested that the response of ζ_D to varying pH of $CaCl_2$ solution was different to that of $MgCl_2$, and they attributed this difference to a higher activity of Mg^{2+} towards the mineral surface compared with Ca^{2+} at elevated temperature, i.e. fully hydrated Mg^{2+} at ambient temperature has larger diameter than Ca^{2+} making the latter to be closer to the mineral surface and thus more active [62], but at higher temperatures it becomes smaller by losing hydration shells at a higher rate, approaches the mineral surface closer and becomes more active. We did not observe any difference in response of ζ_D to varying pH of either solution at elevated temperature, but we only investigated temperatures of 23 °C and 40 °C whilst the data presented by Vinogradov et al. [40] included experiments conducted at 70 °C and 120 °C where the split in response of ζ_D to pH for $CaCl_2$ and $MgCl_2$ was observed. Using Eqs. (3) and (4) allows to accurately predict the expected zeta potential as a function of pH for single salt electrolytes. However, additional work is

required to investigate whether the proposed trends can be interpolated for mixtures of different salts.

To validate the proposed correlations between water pH and the zeta potential (Eqs. (3) and (4)) we compared the values computed using these equations against previously published experimental data. Walker and Glover [32] obtained over 100 zeta potential measurements on intact Fontainebleau sample (F3Q) at 23 °C at reported pH of 6.48 and ambient pressure (i.e., atmospheric content of dissolved CO_2, hence dead water). From the entire NaCl salinity range tested by Walker and Glover [32], the closest to the ionic strength tested in this study was 0.062 M, for which Walker and Glover [32] reported the measured zeta potential of −18 ± 1 mV. Using Eq. (3) and pH of 6.48 [32] the calculated $\zeta_M = -18.92$ mV, which lies within the experimental uncertainty and consistent with the value of −18 mV predicted by the pH dependence of the zeta potential model [63].

Another study that reported measurements of the zeta potential in intact sandstone samples saturated with 0.01 M dead NaCl was published by Vinogradov and Jackson [16]. In that study the authors reported pH of 6.75 ± 0.03 measured in experiments with St Bees1, St Bees 2, Doddington and Stainton samples at 22 ± 1 °C. For all four sandstone samples saturated with 0.01 M dead NaCl at ambient pressure the reported zeta potential was −22 ± 0.4 mV. Using our regression for pH dependence of the zeta potential defined by Eq. (3), the estimated value was found to be −20.24 mV thus validating our approach.

To confirm our proposed model for ζ_D obtained with dead solutions, we compared predictions on the zeta potential made using Eq. (4) against published experimental data [64] obtained with Berea sandstone saturated with 10^{-3} M $CaCl_2$ and $MgCl_2$ solutions at pH between 6.0 and 7.5. Our model yields ζ_D for both solutions between −13.06 mV and −15.09 mV (depending on the used pH value) compared with −9.3 mV and −6.6 mV reported by Thanh and Sprik [64] for $MgCl_2$ and $CaCl_2$, respectively. The values obtained using Eq. (4) are more negative in comparison to those measured by Thanh and Sprik [64] and we attribute this difference to presence of clay minerals in the work of Thanh and Sprik [64], which are known to be more reactive towards divalent cations. On the other hand, the zeta potential reported in the same paper for 10^{-3} M NaCl and Na_2SO_4 at pH between 6.0 and 7.5 was also compared against our model (Eq. (3)). Our prediction for ζ_M was found to be in the range between −16.59 mV and −23.88 mV (corresponding to pH range), which is in a good agreement with the reported by Thanh and Sprik [64] values of −23.9 mV and 24.4 mV for NaCl and Na_2SO_4, respectively.

3.3. Live water zeta potential

Due to initial mixing of 400 mL of live water with 30 mL of dead water, the resulting pH of all re-equilibrated solutions in this study were approximately 0.8 pH units higher than those measured by Li et al. [65] and Peng et al. [47] for the same pressure.

Increasing pore pressure resulted in increased CO_2 dissolution and formation of carbonic acid, and thus a decreasing water pH and consequently a more positive zeta potential (Fig. 6a). All three zeta potentials measured with NaCl at 4.5 MPa, 7.5 MPa and 10 MPa linearly correlated with the corresponding water pH, with the slope of the linear regression (Eq. (5)), which was significantly different from that obtained with dead Na^+ containing solutions (Eq. (3)). Furthermore, all four salt types tested at 7.5 MPa lied on a linear trendline (Fig. 6b), with the slope consistent with that of Fig. 6a:

$$\zeta_L[mV] = -10.90 \times pH + 26.02; R^2 = 0.988 \quad (5)$$

A summary plot including both, dead and live water solutions, is presented in Fig. 7, which suggests that either: a) Eq. (4) should be used for both dead and live $CaCl_2$/$MgCl_2$ solutions, while Eq. (3) should be used for dead NaCl/Na_2SO_4 and Eq. (5) should be used for live NaCl/Na_2SO_4 solutions; or alternatively b) Eq. (5) should be used for all types of live solutions (green regression in Fig. 7) while Eqs. (3) and (4) should be used for dead NaCl/Na_2SO_4 and $CaCl_2$/$MgCl_2$ solutions, respectively.

All of the regressions proposed here for dead and live water solutions (Eqs. (3)–(5)) appear to have a non-zero intercept with the horizontal axis, which is defined as the Isoelectric Point (IEP) that identifies the value of pH that results in a zero zeta potential. For the experiments with dead NaCl and Na_2SO_4 solutions, the IEP is calculated using Eq. (3) and equals 2.59, while the corresponding value for all live water solution calculated using Eq. (5) is 2.39. Both values are consistent with a published study that reported

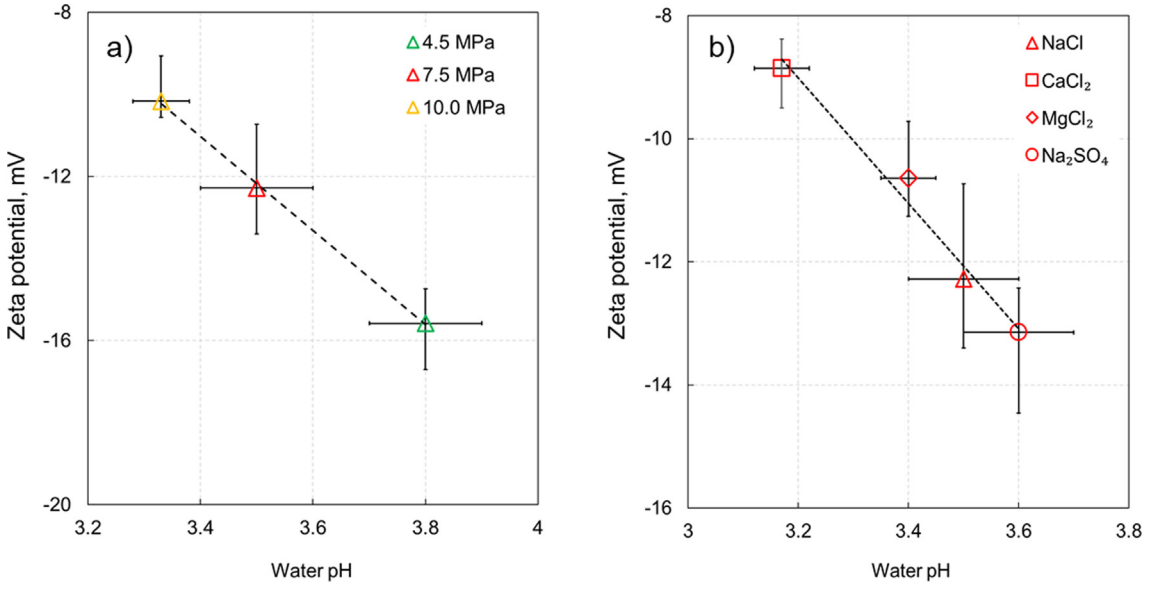

Fig. 6. Zeta potential as a function of live water pH for a) NaCl solutions (with varying pore pressure and therefore different amount of dissolved CO_2) and b) all salt types at pore pressure of 7.5 MPa. All data were measured at 40 °C. The linear regressions in both figures correspond to Eq. (5).

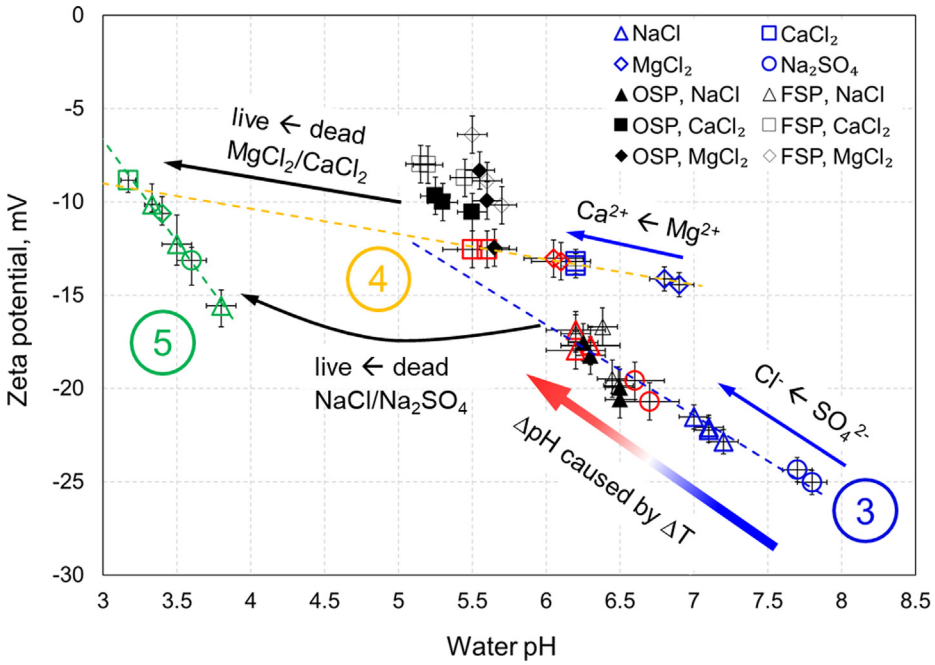

Fig. 7. Zeta potentials measured versus pH of dead and live aqueous solutions. Our data across all pore pressures, temperatures and salt types are shown in color. Literature data for Ottawa and Fontainebleau sandpacks (OSP and FSP, respectively) saturated with 0.015 M dead water [40] are shown in black. The blue and red symbols correspond to 23 °C and 40 °C, respectively. The blue and yellow trendlines are the same as in Fig. 5 and correspond to Eqs. (3) and (4), respectively. The green trendline is identified for all dead water data and given by Eq. (5). The arrows are added to explain the mechanisms of the zeta potential variation along and/or between the trendlines. (For interpretation of the references to color in this figure legend, the reader is referred to the web version of this article.)

IEP for quartz and NaCl to be in the range between pH2.2 and pH2.5 [48]. However, the IEP found for $CaCl_2$ and $MgCl_2$ (Eq. (4)) appears to be at pH of −3.67, which is inconsistent with all previously published results. Therefore, we hypothesize that the regression for pH dependence of the zeta potential with divalent cation salts is not linear throughout the entire range of pH and changes slope at pH around 3.3 where the regression defined by Eq. (4) intersects with the regression given by Eq. (5). This hypothesis is consistent with our results for Na^+ containing solution that appear to switch from the pH dependence defined by Eq. (3) to that given by Eq. (5). Moreover, a published experimental study [66] on crushed Fontainebleau samples saturated with NaCl of resistivity of 100 Ωm (equivalent to ionic strength of 10^{-3} M) demonstrated that pH dependence of the zeta potential was non-uniform. The rate of increase of the measured by Lorne et al. [66] zeta potential with decreasing pH was nearly linear but became significantly steeper below c. pH = 3.5 and had IEP at pH2.5, so that both observations are consistent with our results.

To confirm the pH dependence of ζ_M, ζ_D and ζ_L across the entire pH range, additional experiments at pore pressures that correspond to pH between 4 and 6 for Na^+ containing solutions, and between pH3.5 and pH5.5 for $CaCl_2$ and $MgCl_2$ are required to cover the intermediate pH range. Moreover, additional experiments are also required for all types of solutions at pore pressures that correspond to pH less than 3.2 (i.e., higher partial CO_2 pressure) to investigate the pH dependence of ζ_M and ζ_D under these live water conditions.

4. Implications for CO_2 geological storage

The empirical trends for the zeta potential as a function of water pH (Eqs. (3)–(5)) proposed in this study bear a significant scientific and technological value as they can be used for predicting the expected zeta potential for shallow subsurface settings (low pressure and hence dead water-like behavior of the fluid), as well as for deep formations characterized by high content of dissolved CO_2 (live water-like behavior of the fluid). From the proposed correlations the streaming potential coupling coefficient can be interpreted using Helmholtz-Smoluchowski equation and used for monitoring and characterizing subsurface flows of injected CO_2 or carbonated water during CGS [38]. Moreover, the correlations are important when applied to monitoring movement of water in subsurface settings characterized by variable pH such as hydrocarbon reservoirs (e.g., [15]), groundwater [67,68] or geothermal [69] systems. Our results demonstrate that temperature does not directly affect the zeta potential, instead it affects solubility of CO_2 and pH of aqueous solutions, which in turn impacts the zeta potential. In this sense, laboratory measurements of natural water pH or under varying temperature and CO_2 pressure can be acquired and zeta potential interpreted from the measured values using Eqs. (3)–(5).

Moreover, the proposed empirical correlations for the mineral–water zeta potential can be incorporated in the classical DLVO theory (e.g., [43]) to yield system's wettability thus quantifying the potential of residual trapping of CO_2 during geological sequestration in sandstone formations. For instance, our results suggest that higher reservoir pressure that corresponds to enhanced CO_2 dissolution will results in lower pH and smaller in magnitude rock-water zeta potential thus implying a smaller electrostatic component of the disjoining pressure and hence, less water-wet conditions. In such case, pure sandstone reservoirs (>95% quartz) might be deemed inappropriate for CO_2 injection for geological storage and other formations containing more clays, which are known to make zeta potential larger in magnitude (compare the reported zeta potential measured on Buff Berea, Grey Berea and Parker sandstones saturated with 0.5% NaCl, $CaCl_2$ and $MgCl_2$ in Shehata and Nasr-El-Din [70], to be considered. On the other hand, our results suggest that residual CO_2 trapping controlled by wettability can potentially be improved by making the rock more water-wet via injection of NaCl or Na_2SO_4 rich water of low salinity prior to injecting CO_2 for geological storage. Such procedure would lead to a larger in magnitude negative zeta potential at rock-water

interface, so that the shift towards more water-wet conditions would occur assuming that the zeta potential at CO_2-water interface is also negative.

Furthermore, higher CO_2 pressure, and therefore, higher dissolved CO_2 concentration, causes the equilibrium pH to decrease thus also affecting the mineralization of carbonate and therefore, the CO_2 ultimate storage capacity [71–73].

Despite the fact that our results have been able thus far to accurately predict zeta potential under ambient and supercritical CO_2 conditions, additional experiments are required to quantify the pH dependence of the zeta potential for intermediate pH range of 4.0–5.5 for all types of salts. Additional work is also required to test the pH dependence of the zeta potential for pH < 3, for mixtures of salts to replicate complex natural aqueous solutions that saturate geological porous media, as well as for higher ionic strength solutions typically found in deep sandstone formations such as deep saline aquifers or depleted hydrocarbon reservoirs.

5. Conclusions

We have developed the experimental methodology and for the first time successfully carried out the streaming potential measurements in intact sandstone sample saturated with CO_2-rich aqueous solutions of 0.05 M ionic strength under high pressure (up to 10 MPa) and elevated temperature (up to 40 °C) conditions. For the first time, all streaming potential measurements on silica in contact with aqueous solutions fully equilibrated with CO_2 (live water experiments) were obtained at equilibrium conditions of pressure and temperature that correspond to CO_2 at supercritical state. The zeta potential was carefully interpreted from the measurements and we found that:

1. The zeta potential for all tested solutions, pressure and temperature was negative, which implied that the electrical charge at rock-water interface was always negative and non-zero.
2. The zeta potential of all dead solutions was found to be independent of pore pressure but decreased with increasing temperature; this finding is consistent with previously published data obtained at ambient pressure [40].
3. The zeta potential of all dead solutions was found to be different for NaCl/Na_2SO_4 compared with that of $CaCl_2$/$MgCl_2$.; the finding for Na_2SO_4 is new but the observation for NaCl vs $CaCl_2$/$MgCl_2$ is consistent with the reported results [40].
4. The negative zeta potential of all live solutions decreased in magnitude with increasing pore pressure, reflecting the effect of enhanced CO_2 dissolution under high pressure, which caused pH to decrease; the effect of CO_2 dissolution on the zeta potential has been quantified for the first time in this study.
5. Our results indicate that pH of dead and live solutions is the only control of the zeta potential so that salt type, pore pressure and temperature indirectly affect it via having an impact on pH.
6. We proposed three linear empirical correlations with a high coefficient of determination ($R^2 > 0.97$) to predict the zeta potentials as a function of water pH. The correlations reflect a different response of the zeta potential to presence of mono- or divalent cations in dead solutions, and a distinctly different response to the live water conditions. The correlation for the live water is the first of a kind, thus providing a good source for validating surface complexation models for silica in contact with carbonated aqueous solutions at supercritical CO_2 conditions.
7. The proposed correlations were validated against published experimental data and were confirmed to accurately predict the zeta potential of dead solutions. The isoelectric point predicated by our live water correlation was found to be similar to that published for dead water solutions [48].
8. Our novel results have significant implications for many subsurface settings where high concentration of dissolved CO_2 is expected. Potential applications include management of aquifers, geothermal sources and CGS. Moreover, an improved understanding of the zeta potential of silica-water systems under supercritical CO_2 conditions resulting from this study will inform future studies on thermodynamics of wettability [43], colloid stability and use of nanoparticles [74].

Future experimental work will aim at acquiring zeta potential values in systems comprising clayey sandstones, CO_2-rich aqueous solutions with pH between 4.0 and 5.5, CO_2 pressure higher than 10 MPa that corresponds to pH below 3, ionic strength higher than 0.1 M, and complex background solutions. Moreover, the planned experimental work will investigate impact of grain size, shape, packing and roughness on the zeta potential as well as alternative experimental methods [75]. These experiments will complement the data reported here and expand the range of tested conditions not covered in this work, thus further improving our understanding of the zeta potential at the silica-water interfaces under conditions relevant to CGS. The results will also be used to inform future surface complexation and molecular dynamics simulation studies aimed at describing silica-water-CO_2 systems under CSG conditions.

CRediT authorship contribution statement

Miftah Hidayat: Formal analysis, Investigation, Validation, Visualization, Writing – original draft, Writing – review & editing. **Mohammad Sarmadivaleh:** Resources, Project administration, Supervision, Writing – review & editing. **Jos Derksen:** Supervision, Writing – review & editing. **David Vega-Maza:** Supervision. **Stefan Iglauer:** Funding acquisition, Supervision, Writing – review & editing. **Jan Vinogradov:** Conceptualization, Formal analysis, Resources, Funding acquisition, Methodology, Project administration, Supervision, Validation, Visualization, Writing – original draft, Writing – review & editing.

Declaration of Competing Interest

The authors declare that they have no known competing financial interests or personal relationships that could have appeared to influence the work reported in this paper.

Acknowledgements

Miftah Hidayat was supported by the Aberdeen-Curtin PhD studentship. David Vega-Maza is funded by the Spanish Ministry of Science, Innovation and Universities (“Beatriz Galindo Senior” fellowship BEAGAL18/00259). The authors would also like to thank the Edith Cowan University for funding the design, manufacturing and testing of the experimental setup through RG14747 research grant awarded to the University of Aberdeen.

Appendix A. Supplementary data

Supplementary data to this article can be found online at https://doi.org/10.1016/j.jcis.2021.09.076.

References

[1] A.B. Ronov, A.A. Yaroshevsky, Chemical composition of the earth’s crust, earth’s crust up, Mantle (1969) 37–57, https://doi.org/10.1029/GM013p0037.
[2] W.M. Edmunds, P.L. Smedley, Residence time indicators in groundwater: the East Midlands Triassic sandstone aquifer, Appl. Geochem. 15 (6) (2000) 737–752, https://doi.org/10.1016/S0883-2927(99)00079-7.

[3] W.M. Edmunds, A.H. Bath, D.L. Miles, Hydrochemical evolution of the East Midlands Triassic sandstone aquifer, England, Geochim. Cosmochim. Acta 46 (11) (1982) 2069–2081, https://doi.org/10.1016/0016-7037(82)90186-7.
[4] M.R. Coop, S.M. Willson, Behavior of hydrocarbon reservoir sands and sandstones, J. Geotech. Geoenvironmental Eng. 129 (11) (2003) 1010–1019, https://doi.org/10.1061/(ASCE)1090-0241(2003)129:11(1010).
[5] M.Y. Gulamali, E. Leinov, M.D. Jackson, Self-potential anomalies induced by water injection into hydrocarbon reservoirs, Geophysics. 76 (2011) F283–F292, https://doi.org/10.1190/1.3596010.
[6] L. Aquilina, H. Pauwels, A. Genter, C. Fouillac, Water-rock interaction processes in the Triassic sandstone and the granitic basement of the Rhine Graben: geochemical investigation of a geothermal reservoir, Geochim. Cosmochim. Acta 61 (20) (1997) 4281–4295, https://doi.org/10.1016/S0016-7037(97)00243-3.
[7] R.B. Schmidt, K. Bucher, K. Drüppel, I. Stober, Experimental interaction of hydrothermal Na-Cl solution with fracture surfaces of geothermal reservoir sandstone of the Upper Rhine Graben, Appl. Geochem. 81 (2017) 36–52, https://doi.org/10.1016/j.apgeochem.2017.03.010.
[8] W. Daily, A. Ramirez, D. LaBrecque, J. Nitao, Electrical resistivity tomography of vadose water movement, Water Resour. Res. 28 (5) (1992) 1429–1442, https://doi.org/10.1029/91WR03087.
[9] R.D. Ogilvy, P.I. Meldrum, O. Kuras, P.B. Wilkinson, J.E. Chambers, M. Sen, A. Pulido-Bosch, J. Gisbert, S. Jorreto, I. Frances, P. Tsourlos, Automated monitoring of coastal aquifers with electrical resistivity tomography, Near Surf. Geophys. 7 (5-6) (2009) 367–376, https://doi.org/10.3997/1873-0604.2009027.
[10] M.W. Haartsen, S.R. Pride, Electroseismic waves from point sources in layered media, J. Geophys. Res. Solid Earth. 102 (B11) (1997) 24745–24769, https://doi.org/10.1029/97JB02936.
[11] L. Jouniaux, F. Zyserman, A review on electrokinetically induced seismo-electrics, electro-seismics, and seismo-magnetics for Earth sciences, Solid Earth 7 (2016) 249–284, https://doi.org/10.5194/se-7-249-2016.
[12] R. Peng, B. Di, P.W.J. Glover, J. Wei, P. Lorinczi, Z. Liu, H. Li, Seismo-electric conversion in shale: experiment and analytical modelling, Geophys. J. Int. 223 (2020) 725–745, https://doi.org/10.1093/gji/ggaa288.
[13] L. Jouniaux, A. Maineult, V. Naudet, M. Pessel, P. Sailhac, Review of self-potential methods in hydrogeophysics, Comptes Rendus Geosci. 341 (10-11) (2009) 928–936, https://doi.org/10.1016/j.crte.2009.08.008.
[14] A. Revil, A. Jardani, The Self-Potential Method: Theory and Applications in Environmental Geosciences, Cambridge University Press, Cambridge, 2013. DOI: 10.1017/CBO9781139094252.
[15] M.D. Jackson, M.Y. Gulamali, E. Leinov, J.H. Saunders, J. Vinogradov, Spontaneous potentials in hydrocarbon reservoirs during waterflooding: application to water-front monitoring, SPE J. 17 (2012) 53–69, https://doi.org/10.2118/135146-PA.
[16] J. Vinogradov, M.D. Jackson, Zeta potential in intact natural sandstones at elevated temperatures, Geophys. Res. Lett. 42 (15) (2015) 6287–6294, https://doi.org/10.1002/2015GL064795.
[17] C. Vogt, N. Klitzsch, V. Rath, On self-potential data for estimating permeability in enhanced geothermal systems, Geothermics 51 (2014) 201–213, https://doi.org/10.1016/j.geothermics.2014.01.008.
[18] D. Jougnot, D. Roubinet, L. Guarracino, A. Maineult, Modeling Streaming Potential in Porous and Fractured Media, Description and Benefits of the Effective Excess Charge Density Approach., in: A. Biswas, S.P. Sharma (Reds), Adv. Model. Interpret. Near Surf. Geophys., Springer International Publishing, 2020: bll 61–96. 10.1007/978-3-030-28909-6_4.
[19] R.J. Hunter, Zeta Potential in Colloid Science: Principles and Applications, Academic press, New York, 1981.
[20] A. Revil, P.A. Pezard, P.W.J. Glover, Streaming potential in porous media: 1. Theory of the zeta potential, J. Geophys. Res. Solid Earth 104 (B9) (1999) 20021–20031, https://doi.org/10.1029/1999JB900089.
[21] H. Collini, S. Li, M.D. Jackson, N. Agenet, B. Rashid, J. Couves, Zeta potential in intact carbonates at reservoir conditions and its impact on oil recovery during controlled salinity waterflooding, Fuel 266 (2020), https://doi.org/10.1016/j.fuel.2019.116927 116927.
[22] C.H. Pentland, R. El-Maghraby, S. Iglauer, M.J. Blunt, Measurements of the capillary trapping of super-critical carbon dioxide in Berea sandstone, Geophys. Res. Lett. 38 (2011), https://doi.org/10.1029/2011GL046683.
[23] D.W. Green, G.P. Willhite, Enhanced oil recovery, Henry L. Doherty Memorial Fund of AIME, Society of Petroleum Engineers, Richardson, TX, 1998.
[24] S. Iglauer, M. Ali, A. Keshavarz, Hydrogen Wettability of Sandstone Reservoirs: Implications for Hydrogen Geo-Storage e2020GL090814, Geophys. Res. Lett. 48 (2021), https://doi.org/10.1029/2020GL090814.
[25] G.J. Hirasaki, Wettability: fundamentals and surface forces, SPE Form. Eval. 6 (1991) 217–226, https://doi.org/10.2118/17367-PA.
[26] M.D. Jackson, D. Al-Mahrouqi, J. Vinogradov, Zeta potential in oil-water-carbonate systems and its impact on oil recovery during controlled salinity water-flooding, Sci. Rep. 6 (2016) 1–13, https://doi.org/10.1038/srep37363.
[27] J.N. Israelachvili, The nature of van der waals forces, Contemp. Phys. 15 (2) (1974) 159–178, https://doi.org/10.1080/00107517408210785.
[28] J.H. Adair, E. Suvaci, J. Sindel, Surface and Colloid Chemistry, in: K.H.J. Buschow, R.W. Cahn, M.C. Flemings, B. Ilschner, E.J. Kramer, S. Mahajan, P.B.T.-E. of M.S. and T. Veyssière (Reds), Elsevier, Oxford, 2001: bll 1–10. 10.1016/B0-08-043152-6/01622-3.
[29] Rahul Prasanna Misra, J. Pedro de Souza, Daniel Blankschtein, Martin Z. Bazant, Theory of surface forces in multivalent electrolytes, Langmuir 35 (35) (2019) 11550–11565, https://doi.org/10.1021/acs.langmuir.9b0111010.1021/acs.langmuir.9b01110.s001.
[30] A.V. Delgado, F. González-Caballero, R.J. Hunter, L.K. Koopal, J. Lyklema, Measurement and interpretation of electrokinetic phenomena, J. Colloid Interface Sci. 309 (2) (2007) 194–224, https://doi.org/10.1016/j.jcis.2006.12.075.
[31] A. Alroudhan, J. Vinogradov, M.D. Jackson, Zeta potential of intact natural limestone: Impact of potential-determining ions Ca, Mg and SO_4, Colloids Surf. A Physicochem. Eng. Asp. 493 (2016) 83–98, https://doi.org/10.1016/j.colsurfa.2015.11.068.
[32] E. Walker, P.W.J. Glover, Measurements of the relationship between microstructure, pH, and the streaming and zeta potentials of sandstones, Transp. Porous Media 121 (2018) 183–206, https://doi.org/10.1007/s11242-017-0954-5.
[33] E. Walker, P.W.J. Glover, J. Ruel, A transient method for measuring the DC streaming potential coefficient of porous and fractured rocks, J. Geophys. Res. Solid Earth 119 (2014) 957–970, https://doi.org/10.1002/2013JB010579.
[34] J. Vinogradov, M.Z. Jaafar, M.D. Jackson, Measurement of streaming potential coupling coefficient in sandstones saturated with natural and artificial brines at high salinity, J. Geophys. Res. Solid Earth 115 (2010), https://doi.org/10.1029/2010JB007593.
[35] H. Collini, M. Jackson, Zeta Potential of the Crude Oil-Brine Interface and Implications for Controlled Salinity Waterflooding, in: IOR 2021, European Association of Geoscientists & Engineers, 2021: bll 1–12. Doi: 10.3997/2214-4609.202133090.
[36] J. Vinogradov, M.D. Jackson, Multiphase streaming potential in sandstones saturated with gas / brine and oil / brine during drainage and imbibition, Geophys. Res. Lett. 38 (2011) L01301, https://doi.org/10.1029/2010GL045726.
[37] Mi-Sug Kim, Dong-Heui Kwak, Effect of zeta potential on collision-attachment coefficient and removal efficiency for dissolved carbon dioxide flotation, Environ. Eng. Sci. 34 (4) (2017) 272–280, https://doi.org/10.1089/ees.2016.0325.
[38] J.R. Moore, S.D. Glaser, H.F. Morrison, G.M. Hoversten, The streaming potential of liquid carbon dioxide in Berea sandstone, Geophys. Res. Lett. 31 (2004) L17610, https://doi.org/10.1029/2004GL020774.
[39] A. Liebscher, S. Martens, F. Moller, M. Kuhn, On-shore CO2 storage at the Ketzin pilot site in Germany, in: J. Gluyas, S.B.T.-G.S. of C.D. (CO2) Mathias (Reds), Woodhead Publishing, 2013: bll 278–300. 10.1533/9780857097279.3.278.
[40] J. Vinogradov, M.D. Jackson, M. Chamerois, Zeta potential in sandpacks: Effect of temperature, electrolyte pH, ionic strength and divalent cations, Colloids Surf. A Physicochem. Eng. Asp. 553 (2018) 259–271, https://doi.org/10.1016/j.colsurfa.2018.05.048.
[41] IPCC, IPCC special report on carbon dioxide capture and storage, Cambridge University Press, Cambridge, 2005.
[42] S. Iglauer, Optimum storage depths for structural CO_2 trapping, Int. J. Greenh. Gas Control. 77 (2018) 82–87, https://doi.org/10.1016/j.ijggc.2018.07.009.
[43] Tetsu K. Tokunaga, DLVO-based estimates of adsorbed water film thicknesses in geologic CO_2 reservoirs, Langmuir 28 (21) (2012) 8001–8009, https://doi.org/10.1021/la2044587.
[44] T.W. Kim, T.K. Tokunaga, D.B. Shuman, S.R. Sutton, M. Newville, A. Lanzirotti, Thickness measurements of nanoscale brine films on silica surfaces under geologic CO_2 sequestration conditions using synchrotron X-ray fluorescence, Water Resour. Res. 48 (2012), https://doi.org/10.1029/2012WR012200.
[45] John Gregory, Interaction of unequal double layers at constant charge, J. Colloid Interface Sci. 51 (1) (1975) 44–51, https://doi.org/10.1016/0021-9797(75)90081-8.
[46] K. Adamczyk, M. Prémont-Schwarz, D. Pines, E. Pines, E.T.J. Nibbering, Real-time observation of carbonic acid formation in aqueous solution, Science (80-.) 326 (2009) 1690–1694, https://doi.org/10.1126/science.1180060.
[47] C. Peng, J.P. Crawshaw, G.C. Maitland, J.P. Martin Trusler, D. Vega-Maza, The pH of CO_2-saturated water at temperatures between 308K and 423K at pressures up to 15MPa, J. Supercrit. Fluids. 82 (2013) 129–137, https://doi.org/10.1016/j.supflu.2013.07.001.
[48] Marek Kosmulski, Edward Mączka, Władysław Janusz, Jarl B Rosenholm, Multiinstrument Study of the Electrophoretic Mobility of Quartz, J. Colloid Interface Sci. 250 (1) (2002) 99–103, https://doi.org/10.1006/jcis.2002.8330.
[49] F. Al Saadi, K.-H. Wolf, C. Van Kruijsdijk, Characterization of fontainebleau sandstone: quartz overgrowth and its impact on pore-throat framework, J. Pet. Environ Biotechnol. 7 (2017) 1–12, https://doi.org/10.4172/2157-7463.1000328.
[50] A. Cherubini, B. Garcia, A. Cerepi, A. Revil, Influence of CO_2 on the electrical conductivity and streaming potential of carbonate rocks, J. Geophys. Res. Solid Earth 124 (10) (2019) 10056–10073, https://doi.org/10.1029/2018JB017057.
[51] S. Li, P. Leroy, F. Heberling, N. Devau, D. Jougnot, C. Chiaberge, Influence of surface conductivity on the apparent zeta potential of calcite, J. Colloid Interface Sci. 468 (2016) 262–275, https://doi.org/10.1016/j.jcis.2016.01.075.
[52] R.M. El-Maghraby, C.H. Pentland, S. Iglauer, M.J. Blunt, A fast method to equilibrate carbon dioxide with brine at high pressure and elevated temperature including solubility measurements, J. Supercrit. Fluids 62 (2012) 55–59, https://doi.org/10.1016/j.supflu.2011.11.002.
[53] P.W.J. Glover, Geophysical properties of the near surface earth: electrical properties, Treatise Geophys. 11 (2015) 89–137, https://doi.org/10.1016/B978-0-444-53802-4.00189-5.
[54] L. Jouniaux, J.P. Pozzi, Streaming potential and permeability of saturated sandstones under triaxial stress: consequences for electrotelluric anomalies

prior to earthquakes, J. Geophys. Res. Solid Earth 100 (1995) 10197–10209, https://doi.org/10.1029/95jb00069.
[55] J.H. Saunders, M.D. Jackson, M.Y. Gulamali, J. Vinogradov, C.C. Pain, Streaming potentials at hydrocarbon reservoir conditions, Geophysics 77 (2012) E77–E90, https://doi.org/10.1190/geo2011-0068.1.
[56] Akand W. Islam, Eric S. Carlson, Viscosity models and effects of dissolved CO_2, Energy & Fuels 26 (8) (2012) 5330–5336, https://doi.org/10.1021/ef3006228.
[57] Haining Zhao, Robert M. Dilmore, Serguei N. Lvov, Experimental studies and modeling of CO_2 solubility in high temperature aqueous $CaCl_2$, $MgCl_2$, Na_2SO_4, and KCl solutions, AIChE J. 61 (7) (2015) 2286–2297, https://doi.org/10.1002/aic.v61.710.1002/aic.14825.
[58] H. Zhao, M.V. Fedkin, R.M. Dilmore, S.N. Lvov, Carbon dioxide solubility in aqueous solutions of sodium chloride at geological conditions: experimental results at 323.15, 373.15, and 423.15K and 150bar and modeling up to 573.15K and 2000bar, Geochim. Cosmochim. Acta. 149 (2015) 165–189. Doi: 10.1016/j.gca.2014.11.004.
[59] Yuanhui Liu, Minqiang Hou, Guanying Yang, Buxing Han, Solubility of CO_2 in aqueous solutions of NaCl, KCl, $CaCl_2$ and their mixed salts at different temperatures and pressures, J. Supercrit. Fluids 56 (2) (2011) 125–129, https://doi.org/10.1016/j.supflu.2010.12.003.
[60] D. Al Mahrouqi, J. Vinogradov, M.D. Jackson, Temperature dependence of the zeta potential in intact natural carbonates, Geophys. Res. Lett. 43 (2016) 11578–11587, https://doi.org/10.1002/2016GL071151.
[61] Frank J. Millero, Benjamin DiTrolio, Andres F. Suarez, Gabriele Lando, Spectroscopic measurements of the pH in NaCl brines, Geochim. Cosmochim. Acta 73 (11) (2009) 3109–3114, https://doi.org/10.1016/j.gca.2009.01.037.
[62] S. Datta, A.T. Conlisk, H.F. Li, M. Yoda, Effect of divalent ions on electroosmotic flow in microchannels, Mech. Res. Commun. 36 (1) (2009) 65–74, https://doi.org/10.1016/j.mechrescom.2008.07.006.
[63] P.W.J. Glover, Modelling pH-dependent and microstructure-dependent streaming potential coefficient and zeta potential of porous sandstones, Transp. Porous Med. 124 (2018) 1573–1634, https://doi.org/10.1007/s11242-018-1036-z.
[64] Luong Duy Thanh, Rudolf Sprik, Zeta potential in porous rocks in contact with monovalent and divalent electrolyte aqueous solutions, Geophysics 81 (4) (2016) D303–D314, https://doi.org/10.1190/geo2015-0571.1.
[65] X. Li, C. Peng, J.P. Crawshaw, G.C. Maitland, J.P.M. Trusler, The pH of CO2-saturated aqueous NaCl and NaHCO3 solutions at temperatures between 308 K and 373 K at pressures up to 15 MPa, Fluid Phase Equilib. 458 (2018) 253–263, https://doi.org/10.1016/j.fluid.2017.11.023.
[66] B. Lorne, F. Perrier, J.-P. Avouac, Streaming potential measurements: 1. Properties of the electrical double layer from crushed rock samples, J. Geophys. Res. Solid Earth 104 (1999) 17857–17877, https://doi.org/10.1029/1999JB900156.
[67] M.T. Graham, D.J. MacAllister, J. Vinogradov, M.D. Jackson, A.P. Butler, Self-potential as a predictor of seawater intrusion in coastal groundwater boreholes, Water Resour. Res. 54 (2018) 6055–6071, https://doi.org/10.1029/2018WR022972.
[68] D.J. MacAllister, M.D. Jackson, A.P. Butler, J. Vinogradov, Tidal influence on self-potential measurements, J. Geophys. Res. - Solid Earth 121 (2018) 8432–8452, https://doi.org/10.1002/2016JB013376.
[69] Maria Regina S. Cabahug, Erlindo C. Angcoy, Modeling the reservoir fluids of acidic geothermal wells in Mahanagdong, Leyte, Philippines, Procedia Earth Planet. Sci. 7 (2013) 105–108, https://doi.org/10.1016/j.proeps.2013.03.017.
[70] A.M. Shehata, H.A. Nasr-El-Din, Zeta potential measurements: impact of salinity on sandstone minerals, in: SPE Int. Symp. Oilf. Chem., Society of Petroleum Engineers, Texas, USA, 2015, doi: 10.2118/173763-MS.
[71] Matthew L. Druckenmiller, M. Mercedes Maroto-Valer, Carbon sequestration using brine of adjusted pH to form mineral carbonates, Fuel Process. Technol. 86 (14-15) (2005) 1599–1614, https://doi.org/10.1016/j.fuproc.2005.01.007.
[72] J.P. Kaszuba, D.R. Janecky, M.G. Snow, Carbon dioxide reaction processes in a model brine aquifer at 200 °C and 200 bars: implications for geologic sequestration of carbon, Appl. Geochem. 18 (2003) 1065–1080, https://doi.org/10.1016/S0883-2927(02)00239-1.
[73] John W Morse, Rolf S Arvidson, The dissolution kinetics of major sedimentary carbonate minerals, Earth-Science Rev. 58 (1-2) (2002) 51–84, https://doi.org/10.1016/S0012-8252(01)00083-6.
[74] V. Bueno, A. Bosi, T. Tosco, S. Ghoshal, Mobility of solid and porous hollow SiO_2 nanoparticles in saturated porous media: impacts of surface and particle structure, J. Colloid Interface Sci. 606 (2022) 480–490, https://doi.org/10.1016/j.jcis.2021.07.142.
[75] R. Peng, B. Di, P.W.J. Glover, J. Wei, P. Lorinczi, P. Ding, Z. Liu, Y. Zhang, M. Wu, The effect of rock permeability and porosity on seismo-electric conversion: experiment and analytical modelling, Geophys J. Int. 219 (1) (2019) 328–345, https://doi.org/10.1093/gji/ggz249.